New symmetric and asymmetric supercapacitors based on high surface area porous nickel and activated carbon

V. Ganesh [a], S. Pitchumani [b] and V. Lakshminarayanan [a,*]

[a] *Raman Research Institute, C.V. Raman Avenue, Sadashivanagar, Bangalore-560080, India.*

[b] *Central Electrochemical Research Institute, Karaikudi-630006, India.*

Abstract

We have studied some supercapacitor cell assemblies based on high surface area nickel and nickel oxide materials. Both symmetric and asymmetric configurations consisting of nickel and nickel oxide with activated carbon as a negative electrode have been investigated. A single electrode specific capacitance value of 473 F g^{-1} of nickel is obtained for the porous nickel. We have used cyclic voltammetry (CV), electrochemical impedance spectroscopy (EIS) and charge-discharge profile analysis to characterize the supercapacitor cell assemblies. Based on the analysis of impedance data in terms of complex capacitance and complex power, the relaxation time constant (τ_0) was calculated for different supercapacitor cell assemblies. The quick response time (of the order of milliseconds) with fast energy delivery at relatively high power suggests that these materials can find applications in short time pulse devices. A coulombic efficiency of 0.93 to 0.99 is obtained for the supercapacitor cell assemblies studied in this work. The measured equivalent series resistance (ESR) value is relatively high due to the contribution from the resistance offered by the pores and the contact resistance arising from the cell fabrication method. Although the specific capacitance values are relatively less, the cell exhibits a fast response time, which is a desirable property in certain specialized applications.

Keywords: Supercapacitor; Symmetric and asymmetric cell assemblies; ESR; EDR; Relaxation time constant; Coulombic efficiency; Complex capacitance; Complex power.

* Corresponding Author: Tel.: +91-080-23610122; fax: +91-080-23610492.

E-mail address: narayan@rri.res.in (V. Lakshminarayanan)

1. Introduction

The current research and development efforts on electrochemical power sources are mainly focused on fuel cells, batteries and electrochemical capacitors (EC) and are directed towards achieving high specific energy, high specific power, long cycle life etc., at relatively low cost [1,2]. Due to their high specific power, supercapacitors can find applications in space and automobile (for acceleration and for recuperation of brake energy) technologies [3,4]. A hybrid power source consisting of supercapacitor in parallel configuration to battery is proposed for applications in short duration pulse devices that require high specific power [5,6]. While a battery is a high energy and low power device, which is extensively used in conventional applications, the supercapacitor acts as a low energy and high power device and is ideal for use in high power pulse requirements [7]. Unlike a battery, supercapacitors possess a high power density

with longer cycle-life time. They fill the gap between the batteries and conventional dielectric capacitors as can be observed in the Ragone plots [3,8]. They also cover a wide range of specific energy density ranging from 0.05 Wh kg^{-1} to 15 Wh kg^{-1} and a specific power density from 10 W kg^{-1} to 10^6 W kg^{-1} [3]. Very large capacitance of these devices arises from double layer charging process at the electrode | electrolyte interface. Alternatively, a fast reversible faradaic reaction occurring at or near the electrode surface can also contribute to the overall capacitance, which is known as pseudocapacitance. In literature, three different kinds of supercapacitors based on carbon-carbon [9,10], transition metal oxides [11,12] and conducting polymers [13-15] have been reported.

Electrochemical double layer capacitors (EDLC) use high surface area carbon materials such as activated carbon, carbon fiber cloth, carbon aerogels and foams as the electro active materials. A double layer capacitance of about 40 μF cm^{-2}, which corresponds to a specific capacitance of 100-150 F g^{-1} was earlier reported [8,16]. The high specific capacitance values arise from the high surface area of these materials. Since the micropores of <2nm size cannot be wetted by the electrolyte, a significant fraction of the total area is inaccessible to the electrolyte, which limits its capacitance. To some extent, the wettability and accessibility can be improved by the use of conducting polymer depending upon the size of the pores present within the polymer matrix [14]. In this case, the

overall measured capacitance arises mainly from the pseudocapacitance contribution due to the redox reaction of conducting polymers [13-15]. RuO_2 and IrO_2 exhibit pseudocapacitance behaviour and have huge specific capacitance values ranging from 720-760 F g^{-1} (for single electrode) as supercapacitors [17]. However, the high cost of these materials limits its prospects of large-scale commercialization. There are reports in the literature based on nickel oxide [18-21], cobalt oxide [22] and manganese oxide [23] supercapacitors, which are inexpensive and exhibit pseudocapacitive behaviour similar to that of ruthenium oxide.

We find from the literature that there are several reports on nickel oxide as supercapacitor electrode material, which have specific capacitance values ranging from 240-277 F g^{-1} (for single electrode) [18-21]. The preparation of NiO involves either sol-gel technique or electrochemical deposition followed by heat treatment in air at around 300^0C. There are studies on the effect of heat treatment, electrolyte environment and the potential range of operation on the measured capacitance values of nickel oxide electrodes. Park et al. reported an electrochemical capacitor based on a $Ni(OH)_2$/activated carbon composite electrode with a specific capacitance value of 530 F g^{-1} (for single electrode) [24]. Nelson and Owen reported a supercapacitor/battery hybrid system based on the template deposited mesoporous $Ni/Ni(OH)_2$ positive electrode and a palladium

negative electrode [25]. Bursell et al. reported a hybrid supercapacitor based on ultrathin film of nickel [26], which indicates that the Ni electrodes have been considered as the positive electrode in asymmetric supercapacitors. Since both the double layer capacitance and pseudocapacitance are interfacial phenomena, the materials used for supercapacitors should possess a high specific surface area with good wettability of electrolyte to enhance their charge storage capability. Recently, we reported a method for the preparation of a high surface area porous nickel material by template electrodeposition using a hexagonal lyotropic liquid crystalline phase as a template [27], which was shown to be a potential candidate for supercapacitor electrode material [28].

In this paper, we report some new symmetric and asymmetric supercapacitor cell assemblies based on the high surface area porous nickel and NiO electrodes with activated carbon as a negative electrode. The high surface area porous nickel material is obtained by template electrodeposition and the nickel oxide electrode is derived from the electrochemical oxidation of porous nickel [27]. We have used electrochemical techniques such as cyclic voltammetry (CV), electrochemical impedance spectroscopy (EIS) and charge-discharge transient analysis for the characterization of supercapacitors. EIS data were analyzed in terms of complex power and complex capacitance values to determine the relaxation time constant (τ_0) and the figure of merit of supercapacitors. The

charge-discharge profiles were used to calculate various parameters such as specific energy (SE), specific power (SP), specific capacitance (SC), columbic efficiency (η) and equivalent series resistance (ESR).

2. Experimental

High surface area porous nickel material was prepared from a new hexagonal liquid crystalline phase consisting of 42 wt% Triton X-100, 5 wt% PAA and 53 wt% water in which the aqueous phase was replaced by nickel sulphamate bath as reported in our previous work [27]. The roughness factor, which is a measure of true surface area of the porous nickel electrode, was determined using cyclic voltammetry in 0.5M NaOH aqueous solution [27]. Activated carbon (Lancaster) having a specific surface area of 1500 m^2 g^{-1} was used as the negative electrode in asymmetric supercapacitor cell assemblies. The carbon paste was prepared using N-methylpyrolidine as a binder and pasted onto a smooth nickel support that acts as a current collector. This carbon paste electrode was heated in an oven at around 100^0C for about 15 minutes and then allowed to cool down to room temperature. Polypropylene membrane of thickness 250μm was used as an electrode separator in the cell assemblies.

Electrochemical characterization of template deposited porous nickel electrode material in both the symmetric cell assembly (Porous Ni| KOH |Porous

Ni) and the asymmetric cell assembly (Porous Ni| KOH |Activated carbon) of supercapacitors was carried out using cyclic voltammetry (CV), electrochemical impedance spectroscopy (EIS) and charge-discharge analysis. Cyclic voltammetry was performed in the double layer region of potential ranging from –1.1V to –0.9V in 6M KOH aqueous solution at various potential scan rates. First, the high surface area porous Ni electrode was kept at a potential of –1.6V vs. SCE for 600s in the alkaline solution. This process reduces the surface oxides and cathodically cleans the surface by the evolution of hydrogen gas. This is followed by keeping the electrode at a potential of –1.02V vs. SCE, which oxidizes any metal hydrides on the surface [29]. Finally the supercapacitor cell was scanned in the double layer region to determine the capacitance.

Electrochemical oxidation of porous nickel to nickel oxide had also been carried out to show that NiO obtained from the high surface area porous Ni can also be used as the supercapacitor electrode material. Porous Ni was converted into its corresponding NiO by potential scanning at the nickel oxide region [21,30]. First the potential was cycled between –0.1V and +0.5V vs. SCE in the alkaline solution for more than 25 cycles at various scan rates, where the redox process of NiO formation and its stripping takes place. The capacitance was then determined by scanning the oxidized nickel oxide electrode in the potential range from –0.1V to +0.2V vs. SCE at different scan rates. The potential scan rates used for cyclic

voltammetric experiments were varied from 2 mV s^{-1} to 500 mV s^{-1}. The capacitance was calculated by measuring the current separation (I) from the cyclic voltammogram and the scan rate (ν) using the formula, $C = I/\nu$. Both the symmetric as well as the asymmetric supercapacitor cell assemblies were analyzed.

Electrochemical impedance spectroscopic studies were performed in 6M KOH aqueous solution by applying a sinusoidal signal of 10mV peak-to-peak amplitude at a frequency range of 100mHz to 100kHz. The impedance data were analyzed in terms of complex capacitance and complex power in order to determine the relaxation time constant (τ_0). The charge-discharge analysis was carried out at two different constant current densities of 1 mA cm^{-2} and 4 mA cm^{-2} at a potential range of 0 to 1V for both the symmetric and asymmetric supercapacitor cell assemblies in 6M KOH aqueous solution. All the electrochemical measurements were carried out using an EG&G Electrochemical Impedance Analyzer (model 6310) which can be operated both in dc and ac modes and interfaced to a PC through a GPIB card (National instruments). The charge-discharge analysis was performed in WonATech Automatic Battery Cycler, WBCS 3000 system interfaced to a computer. The analysis of data was carried out using WBCS V3.0 software and different parameters of the supercapacitor cell assemblies were calculated. All the chemical reagents used were AnalaR (AR)

grade. Millipore water having a resistivity of 18 MΩ cm was used in all the experiments performed at room temperature.

3. Results and Discussion

3.1. Cyclic voltammetry

3.1.a. Using the high surface area porous nickel as an electro active material:

Figures 1 (a) and (b) show the cyclic voltammograms of symmetric (Porous Ni| KOH |Porous Ni) and asymmetric (Porous Ni| KOH |Activated carbon) supercapacitor cell assemblies in 6M KOH as the electrolyte. The potential scan rate was varied from 2 mV s^{-1} to 500 mV s^{-1}. It can be seen from the voltammograms that there is a large current separation between the forward and reverse scans with no visible peak formation, indicating a clear capacitive behaviour. It can also be observed that the voltammograms are not symmetrical about the zero current axis. The fact that the voltammograms do not show perfect box type rectangular features with a mirror image characteristic implies that there is a substantial pseudocapacitance contribution to the overall measured capacitance. The capacitance values are determined by measuring the ratio of the magnitude of current separation and the scan rate. The fact that all the CVs show almost rectangular features at 500 mV s^{-1} scan rate with high current density values indicates a good electrochemical activity and high power density. The

unsymmetrical nature of the CVs arises due to a large reduction current owing to nickel hydride (NiH) formation, which is not completely oxidized during the forward cycle. Table 1 shows the double layer capacitance and specific capacitance values of the respective symmetric and asymmetric supercapacitor cell assemblies based on the high surface area porous nickel at different potential scan rates. It can be noted that the capacitance values vary with the scan rate. A maximum capacitance value of 66 mF cm^{-2} is obtained at 100 mV s^{-1} scan rate for the symmetric supercapacitor, which corresponds to a specific capacitance of 22 F g^{-1}. A double layer capacitance of 250 mF cm^{-2} corresponding to a specific capacitance of 84 F g^{-1} is obtained for the asymmetric supercapacitor at 2 mV s^{-1}. These values are quite low compared to a single electrode value of 473 F g^{-1} that we have reported earlier [28]. It is speculated that the high ionic resistance inside the pores leads to a decrease in specific capacitance of the electrode material used in the symmetric cell assembly. The dependence of the measured specific capacitance on the scan rate is due to the contribution from pseudocapacitance arising out of the formation and subsequent oxidation of metal hydrides at this potential range [28].

3.1.b. Using the nickel oxide (NiO) electrode:

Electrochemical oxidation method is employed to convert the high surface area porous nickel to nickel oxide. In this case too both the symmetric (NiO| KOH |NiO) and asymmetric (NiO| KOH |Activated carbon) supercapacitor cell assemblies were investigated. Infact, the supercapacitors based on NiO show a better capacitive behaviour than the porous Ni electrode. Figures 2 (a) and (b) show the cyclic voltammograms of symmetric and asymmetric supercapacitors based on NiO in 6M KOH respectively. It is evident from the cyclic voltammograms that the supercapacitor cell assemblies show a large current separation with a mirror image characteristic especially at higher scan rates indicating a capacitive behaviour. Table 2 shows the double layer capacitance and specific capacitance values of supercapacitors based on NiO, obtained at different potential scan rates. It can be seen that the capacitance values vary with the scan rate and the maximum capacitance value of 15 mF cm^{-2} is obtained at 2 mV s^{-1} for the symmetric supercapacitor, which corresponds to a specific capacitance value of 5 F g^{-1}. A double layer capacitance value of 100 mF cm^{-2} corresponding to a specific capacitance value of 34 F g^{-1} is obtained for the asymmetric supercapacitor at 2 mV s^{-1} scan rate. These values are of course quite less compared to a single electrode capacitance value of 57 F g^{-1} [28]. It can also be noted that the specific capacitance values are very much lower compared to the literature value of 240 to 277 F g^{-1} (for single electrode) and is due to the different

procedures employed to obtain NiO in the present work. It is also felt that the lower values of capacitance obtained by the electrochemical oxidation method in our case may be due to incomplete conversion of nickel to nickel oxide within the pores. We have restricted ourself to the double layer region for the capacitance measurement in order to avoid the contribution from pseudocapacitance arising out of the redox reaction. It can be concluded that the asymmetric cell assembly provides a higher capacitance value in both the cases of porous nickel and NiO electrodes, when compared to symmetric cell assembly.

To verify the pseudocapacitance contribution, we have studied the effect of scan rate on the capacitance of various symmetric and asymmetric supercapacitor cell assemblies based on nickel and nickel oxide electrodes. Figure 3 (a) shows the plot of I/ν vs. scan rate (ν) for the symmetric cell assembly of porous nickel and figure 3 (b) shows the variation of I/ν vs. scan rate (ν) for the other symmetric and asymmetric supercapacitor cell assemblies studied in this work. The specific capacitance increases exponentially with decreasing scan rate except in the case of symmetric porous nickel cell assembly. Similar behaviour is reported in the literature for various electrode materials [31-34]. In the case of RuO_2 supercapacitor [33], this effect is attributed to increasing ionic resistance inside the pores leading to a decrease in its specific capacitance value. A similar effect is believed to occur in the present system where the surface reaction due to

nickel hydride formation contributes the pseudocapacitance. This is also suggested by the scan rate dependence of the specific capacitance. In the case of symmetric porous nickel supercapacitor, the capacitance increases with the scan rate. We felt that at higher scan rates, the pseudocapacitance contribution is dominant over the double layer capacitance due to the high surface area and porous nature of the material.

3.2. Electrochemical impedance spectroscopy

In order to investigate the electrochemical characteristics of the supercapacitor electrodes | electrolyte interface in a quantitative manner, ac impedance spectroscopic measurements were performed. Figures 4 (a) and (b) show the respective Nyquist plots of symmetric and asymmetric supercapacitor cell assemblies based on the high surface area porous nickel and activated carbon in 6M KOH aqueous solution. Inset shows the expanded high frequency region of the same plot. It can be seen from the figures that the cell shows a semi circle at high frequency region and a straight line at lower frequency region. This implies that the supercapacitors show a blocking behaviour at high frequencies and capacitive behaviour at low frequencies. The impedance plots obtained in this case are similar to that of transmission line model (TLM) for the porous electrode proposed by Conway [8,35] for the case of under potential deposition with

continuous reaction. The TLM consists of a parallel combination of R and C elements interconnected with the pore resistance element, R_p. In our case, the contribution from pseudocapacitance due to the nickel hydride redox reaction is dominant at this potential for the porous nickel electrodes, which gives an additional pseudocapacitance element (C_ϕ). The phase angle values close to 65^0 and 70^0 are obtained for the symmetric (Porous Ni| KOH |Porous Ni) and asymmetric (Porous Ni| KOH |Activated carbon) supercapacitors respectively, indicating a dominant capacitive behaviour. Figures 5 (a) and (b) show the respective Nyquist plots of symmetric and asymmetric supercapacitors based on NiO in 6M KOH aqueous solution. The insets of the figures show an expanded high frequency region. It can be inferred form the plots that the supercapacitors show a very small kinetic arc at high frequencies implying the charge transfer controlled regime and a straight line at low frequencies indicating the capacitive regime. A phase angle of 65^0 and 77^0 obtained for the respective symmetric and asymmetric supercapacitors based on NiO electrodes, imply that the material is suitable for the fabrication of low leakage capacitors.

In general, a supercapacitor behaves as a pure resistor at high frequencies and as a capacitor at low frequencies. In the mid frequency range, it behaves as a combination of resistor and capacitor, where the electrode porosity and thickness of electroactive materials play a vital role in the determination of capacitance

values. This is in conformity with the transmission model. The above-mentioned effect shifts the low frequency capacitive behaviour towards the more resistive values along the real axis, from which equivalent distributed resistance (EDR) arising due to the porous nature of the electrode material can be calculated. From the high frequency intercept of the semicircle, the equivalent series resistance (ESR) can be determined. In the present study, ESR value is more due to the additional EDR arising from the resistance offered by the diffusion of ions through the pores, which contributes to the overall resistance value. The utility of the supercapacitors is validated by analyzing the impedance data using complex capacitance and complex power method as reported earlier.

3.2.1. Complex capacitance and Complex power analysis:

The relaxation time constant (τ_0), which is also known as dielectric relaxation time of the supercapacitor [36], corresponds to the figure of merit of the supercapacitor [37]. This parameter represents one of its discharge characteristics. It has been studied for various cell assemblies based on the analysis of complex capacitance and complex power using impedance data by other workers [38,39].

The complex capacitance is expressed as follows,

$$C(\omega) = C'(\omega) - j\, C''(\omega) \qquad (1)$$

where $C'(\omega)$ is the real part of the complex capacitance and $C''(\omega)$ is the imaginary part of the complex capacitance $C(\omega)$ and they are given by ,

$$C'(\omega) = - Z''(\omega) \ / \{\omega |Z(\omega)|^2\} \quad (2)$$

and

$$C''(\omega) = Z'(\omega) \ / \ \{\omega |Z(\omega)|^2\} \quad (3)$$

where $Z'(\omega)$ and $Z''(\omega)$ are the respective real and imaginary parts of the complex impedance $Z(\omega)$. ω is the angular frequency and it is given by $\omega = 2\pi f$.

At low frequency, $C'(\omega)$ corresponds to the capacitance of the electrode material and $C''(\omega)$ corresponds to the energy dissipation by an irreversible process that leads to a hysteresis [39].

The value of complex power can be expressed as,

$$S(\omega) = P(\omega) + j\, Q(\omega) \quad (4)$$

where the real part of the complex power $P(\omega)$ is called the active power and $Q(\omega)$, the imaginary part is called the reactive power, which are given by,

$$P(\omega) = \omega\, C''(\omega) \, |\Delta V_{rms}|^2 \quad (5)$$

and

$$Q(\omega) = -\omega\, C'(\omega) \, |\Delta V_{rms}|^2 \quad (6)$$

where $|\Delta V_{rms}|^2 = \Delta V_{max} / \sqrt{2}$ with V_{max} being the maximal amplitude of the ac signal.

The relaxation time constant, τ_0 ($=1/2\pi f_0$) can be calculated from the plots of $C'(\omega)$ vs. frequency and $C''(\omega)$ vs. frequency. The real part of the complex capacitance $C'(\omega)$ decreases asymptotically with frequency (Figures not shown). This is characteristic of the electrode structure and electrode | electrolyte interface. From the frequency corresponding to the half of the maximum value of $C'(\omega)$, the relaxation time constant (τ_0) can be determined. The change of imaginary part of the complex capacitance $C''(\omega)$ with frequency goes through a maximum at a frequency, f_0, from which the value of τ_0 can be calculated. Figures 6 (a-d) show the variation of $C''(\omega)$ with frequency for the symmetric and asymmetric supercapacitor cell assemblies studied in this work. The plots show a characteristic hysteresis for all the cell assemblies studied. It can be noted that the symmetric and asymmetric cell assemblies based on nickel oxide show a clear peak formation, while the cell assemblies based on porous nickel electrodes have not reached the maximum even at the lowest frequency used in this study.

The plots of normalized power with the frequency shown in figures 7 and 8 represent the relaxation time constants for the respective cell assemblies. The power dissipated into the system can be analyzed from the normalized active power denoted by $|P|/|S|$. At high frequency, when the supercapacitor behaves like a pure resistor, all the power is dissipated into the system (P=100%). However, no power is dissipated into a pure capacitance at low frequency. Infact, the values of

|P|/|S| and |Q|/|S| show opposite trends with frequency as can be seen from the figures 7 and 8. The crossing of two plots occurs at a frequency f_0, known as resonance frequency, from which the relaxation time constant, τ_0 ($=1/2\pi f_0$), can be determined explicitly. This time constant, τ_0 corresponds to a phase angle of 45^0 and it represents the transition of electrochemical capacitor from a purely resistive to a purely capacitive behaviour. For a frequency, $f > 1/\tau_0$, it acts as a pure resistor and for $f < 1/\tau_0$, it behaves as a pure capacitor. In what follows, we discuss the results based on the analysis using complex power method, which is the most appropriate one for evaluating the figure of merit of the supercapacitor cell assemblies.

Figures 7 (a) and (b) show the plots of |P|/|S| and |Q|/|S| of the complex power vs. frequency (in logarithmic scale) for the respective symmetric and asymmetric supercapacitors based on the high surface area porous nickel electrode. These parameters show the expected trends as discussed above. From the crossing of two plots at a frequency, f_0, the value of τ_0 has been calculated. A value of 10ms and 0.16s have been calculated for the respective symmetric (Porous Ni| KOH |Porous Ni) and asymmetric (Porous Ni| KOH |Activated carbon) supercapacitors indicating that the cell based on the symmetric system is able to deliver its stored energy almost ten times faster at a high power. Figures 8 (a) and (b) show the plots of |P|/|S| and |Q|/|S| of the complex power vs. frequency (in logarithmic scale) for

the respective symmetric and asymmetric supercapacitors based on NiO, obtained by electrochemical oxidation of porous Ni electrode. The relaxation time constant (τ_0) values of 650μs and 21ms are determined for the symmetric (NiO| KOH |NiO) and asymmetric (NiO| KOH |Activated carbon) supercapacitor cell assemblies respectively. By comparing the figures 7 and 8 and from the calculated relaxation time constants, it is evident that the response time is faster for the NiO supercapacitors than the porous Ni system, even though the specific capacitance value is higher for the latter. In addition, the symmetric cell assembly provides the faster delivery of stored energy at a much higher power when compared to the asymmetric cell assembly.

3.3. Charge-Discharge profile analysis

In order to evaluate the charge storage capacity, durability of cycle lifetime and various electrical parameters, the galvanostatic charge-discharge analysis of the supercapacitor cell assemblies were performed at two different current densities namely 1 mA cm^{-2} and 4 mA cm^{-2}. The electrical parameters such as specific capacitance (SC), specific power (SP) and specific energy (SE) are calculated using the following relationships [6],

$$SC = [I \times t] / [V \times m] \quad (7)$$

$$SP = [I \times V] / m \quad (8)$$

$$SE = [I \times t \times V] / m \quad (9)$$

where SC is specific capacitance in F g^{-1}, SP is specific power in W g^{-1} and SE is specific energy in Wh g^{-1}. The above expressions show the discharge current (I) in amperes, voltage range (V) in volts, discharge time (t) in seconds and mass of the electroactive material (m) in grams. The coulombic efficiency is calculated using the following equation,

$$\eta = [t_D / t_C] \times 100 \quad (10)$$

where t_C and t_D represent the time of charging and discharging respectively.

Figures 9 (a) and (b) show the typical charge-discharge profiles of the respective symmetric and asymmetric supercapacitor cell assemblies using the high surface area porous nickel electrodes in 6M KOH aqueous solution. We have used a voltage range of 0 to 1V in order to evaluate the performance at higher voltages. It can be seen that the charge-discharge profiles deviate from the typical linear variation of voltage with time normally exhibited by a purely electrochemical double layer capacitors (EDLC). The observed non-linearity in our case can be explained as due to the pseudocapacitance arising out of the redox reaction at this voltage range. It can also be noted that the charging-discharging times are almost the same. For symmetric supercapacitor (Porous Ni| KOH |Porous Ni), a specific capacitance of 23 F g^{-1} is obtained at 4 mA cm^{-2} with a specific power of 1.23 W g^{-1} and a specific energy of 23.31 kWh kg^{-1}. The

specific capacitance value decreases to 50% after 500 cycles. The coulombic efficiency ranges from 0.93 to 0.99. There is a large voltage drop at the beginning of the discharge curve, which is attributed to the resistance arising out of the porous nature of the electrode. For the asymmetric supercapacitor (Porous Ni| KOH |Activated carbon), a specific capacitance of 30 F g^{-1} is obtained at 1 mA cm^{-2} current density with a specific power of 330 W kg^{-1} and a specific energy of 28.88 Wh g^{-1}. In this case also the specific capacitance value decreases to 50% of its original value after 500 cycles. The coulombic efficiency value ranges from 0.91 to 0.97. However, there is no significant voltage drop during the initial stage of the discharge process. Here the variation of voltage with respect to time is again not linear due to the porous nature of the electrode materials, which conforms to the proposed model of Conway and Pell [35]. The equivalent series resistance (ESR) value increases marginally with the number of cycles when activated carbon was used as the negative electrode in the asymmetric supercapacitor.

The high surface area porous nickel was electrochemically oxidized to obtain its corresponding NiO as discussed earlier. Figures 10 (a) and (b) show the representative charge-discharge profiles of both the symmetric and asymmetric supercapacitor cell assemblies based on NiO in 6M KOH aqueous solution respectively. It can be seen that the symmetric NiO cell assembly (Fig. 10(a)),

exhibits a non-linear charge-discharge profile. On the other hand, the asymmetric device (Fig. 10(b)) shows a perfect linear characteristic, implying the formation of good electrode | electrolyte interface with a well-defined conductivity. In addition, no ohmic drop is observed in the case of asymmetric supercapacitor and not quite significant ohmic drop in the case of symmetric cell assembly. We have employed two different current densities for the measurements in which the activated carbon was used as a negative electrode. For the symmetric supercapacitor (NiO| KOH |NiO), a specific capacitance of 37 F g^{-1} is obtained at a constant current density of 4 mA cm^{-2} with a specific power of 1.23 W g^{-1} and a specific energy of 37 Wh g^{-1}. Infact the specific capacitance decreases to a large extent with the number of cycles while the ESR value increases marginally. The coulombic efficiency of the cell ranges from 0.85 to 0.97. For asymmetric supercapacitor (NiO| KOH |Activated carbon), a specific capacitance of 40 F g^{-1} at a constant current density of 1 mA cm^{-2} with a specific power of 330 W kg^{-1} and a specific energy of 35 Wh g^{-1} is obtained. The coulombic efficiency ranges from 0.80 to 0.90. It can be seen that the specific capacitance values measured from the charge-discharge analysis described above for the different supercapacitor cell assemblies are higher than the corresponding values determined from cyclic voltammetry shown in Table 1 and 2. This can be attributed to the different potential ranges used for the capacitance measurement in these two methods. The larger value in the case of

charge-discharge studies arises from the enhanced pseudocapacitance contribution to the total measured capacitance.

Usually, the ESR values for the supercapacitors lie in the range of a few hundreds of milliohms, which arises mainly from the contact and electrolytic resistances. In the case of porous electrodes, the contribution from equivalent distributed resistance (EDR) may also add to the measured ESR value. In the present study, the symmetric supercapacitor (Porous Ni| KOH |Porous Ni) based on the high surface area porous Ni alone shows a higher ESR value ranging from ~10Ω-20Ω, compared to ~1Ω-3Ω of all the other supercapacitor cell assemblies used in this study. The fact that the asymmetric supercapacitor (NiO| KOH |Activated carbon) based on NiO shows almost no voltage drop rules out the contribution from the contact resistance. Obviously, the ESR contribution in other cell assemblies arises from the contact resistance of the respective cell. The higher ESR value in the case of symmetric porous nickel supercapacitor can be attributed to the diffusional resistance (EDR) of the electrolyte inside the pores [40]. We have earlier reported a flooded pear shaped pore model [27] for the porous nickel material. This pore geometry makes it difficult for a free flow of ions, which leads to a large increase in the resistance value. The fact that the asymmetric supercapacitor based on NiO has a very negligible ESR value implies that the geometry of the pores is altered during the process of electrochemical oxidation. It

is felt that this behaviour facilitates better ionic flow within the pores. Inspite of the higher ESR and lower specific capacitance values, these supercapacitors have fast response time, which are well suited for applications in short duration pulse devices.

4. Conclusions

We have studied the symmetric and asymmetric supercapacitor cell assemblies using high surface area porous nickel and nickel oxide as the electrode materials. The specific capacitance values of the devices were measured using cyclic voltammetry and charge-discharge analysis. The specific capacitance values range from 20-40 F g^{-1} and exhibit a frequency dispersion. The devices are shown to be stable for upto 500 charge-discharge cycles. The measured ESR value is relatively high in the case of porous nickel supercapacitors, which can be minimized by optimizing the design of the cell assembly. The relaxation time constant values ranging from 0.65ms to 160ms were determined for different cell assemblies using electrochemical impedance spectroscopy studies. From these studies we find that the symmetric supercapacitor exhibits a faster energy delivery capability at a higher power compared to the asymmetric device. This demonstrates the potential application in short duration pulse devices.

Acknowledgement

We gratefully acknowledge Prof. A.K. Shukla and Dr. N.G. Renganathan, CECRI, Karaikudi for many useful discussions and suggestions. We also thank the research colleagues in the laboratory at CECRI, Karaikudi for their help in some experiments.

Table-1

The double layer capacitance and specific capacitance values of symmetric and asymmetric supercapacitor cell assemblies based on the high surface area porous Ni electrode.

Scan rate ($mV\ s^{-1}$)	Double layer capacitance ($mF\ cm^{-2}$)		Specific capacitance ($F\ g^{-1}$)	
	Ni| KOH |Ni	Ni| KOH |AC*	Ni| KOH |Ni	Ni| KOH |AC*
2	47	250	15.67	84.00
5	13	195	4.33	65.00
10	26	100	8.67	33.33
25	55	172	18.33	57.33
50	61	123	20.33	41.00
100	66	80	22.00	26.67
200	62	39	20.67	13.00
500	61	18	20.33	6.00

*** AC --- Activated carbon**

Table-2

The double layer capacitance and specific capacitance values of symmetric and asymmetric supercapacitor cell assemblies based on NiO obtained from the porous Ni electrode.

Scan rate ($mV\ s^{-1}$)	Double layer capacitance ($mF\ cm^{-2}$)		Specific capacitance ($F\ g^{-1}$)	
	NiO| KOH |NiO	NiO| KOH |AC*	NiO| KOH |NiO	NiO| KOH |AC*
2	15	100	5.00	34.00
5	10	83	3.33	27.67
10	11	51	3.67	17.00
25	12	29	4.00	9.67
50	10	20	3.33	6.67
100	8	12	2.67	4.00
200	6	7	2.00	2.33
500	4	4	1.33	1.33

*** AC --- Activated carbon**

References

1. (a) B.E. Conway, J. Electrochem. Soc., 138 (1991) 1539. (b) B.E. Conway, V. Birss, and J. Wojtowicz, J. Power Sources, 66 (1997) 1.
2. (a) I. Tanahashi, A. Yoshida, and A. Nishino, J. Electrochem. Soc., 137 (1990) 3052. (b) J.P. Zheng and T.R. Jow, J. Electrochem. Soc., 142 (1995) L6.
3. R. Kotz and M. Carlen, Electrochim. Acta, 45 (2000) 2483.
4. E.E. Kalu, T.T. Nwoga, V. Srinivasan, and J.W. Weidner, J. Power Sources, 92 (2001) 163.
5. A.F. Burke, J. Power Sources, 91 (2000) 17.
6. K. Rajendra Prasad and N. Munichandraiah, Electrochem. Solid State Lett., 5, (2002) A271.
7. A. Rudge, J. Davey, I. Raistrick, and S. Gottesfeld, J. Power Sources, 47 (1994) 89.
8. B.E. Conway, Electrochemical Supercapacitors, Kluwer Academic/ Plenum Publishers, New York (1999) pp.1.
9. T. Morimoto, K. Hiratsuka, Y. Sanada, and K. Kurihara, J. Power Sources, 60 (1996) 239.
10. A. Du Pasquier, J.A. Shelburne, I. Plitz, F. Badway, A.S. Gozdz, and G. Amatucci, in Proceedings of the 11th International Seminar on Double Layer Capacitors and Similar Energy Storage Devices, Deerfield Beach, FL, December 3-5, (2001).
11. Q.L. Fang, D.A. Evans, S.L. Roberson, and J.P. Zheng, J. Electrochem. Soc., 148 (2001) A833.
12. I.D. Raistrick and R.T. Sherman, in Electrode Materials and Processes for Energy Conversion and Storage, S. Srinivasan, S. Wagner, and H. Wroblowa, Editors, PV 87-12, The Electrochemical Society Proceedings Series,

Pennington, NJ (1987) pp. 582.

13. A. Laforgue, P. Simon, J.F. Fauvarque, J.F. Sarrau, and P. Lailler, J. Electrochem. Soc., 148 (2001) A1130.
14. M. Mastragostino, C. Arbizzani, R. Paraventi, and A. Zanelli, J. Electrochem. Soc., 147 (2000) 407.
15. A. Di Fabio, A. Giorgi, M. Mastragostino, and F. Soavi, J. Electrochem. Soc., 148 (2001) A845.
16. A.J. Bard, and L.R. Faulkner, Electrochemical Methods: Fundamentals and applications, Wiley, New York, (1980).
17. J.P. Zheng, P.J. Cygan, and T.R. Zow, J. Electrochem. Soc., 142 (1995) 2699.
18. K.C. Liu and M.A. Anderson, J. Electrochem. Soc., 143 (1996) 124.
19. V. Srinivasan and J.W. Weidner, J. Electrochem. Soc., 144 (1997) L210.
20. V. Srinivasan and J.W. Weidner, J. Electrochem. Soc., 147 (2000) 880.
21. K.W. Nam and K.B. Kim, J. Electrochem. Soc., 149 (2002) A346.
22. C. Lin, J.A. Ritter, and B.N. Popov, J. Electrochem. Soc., 145 (1998) 4097.
23. S.C. Pang, M.A. Anderson, and T.W. Chapman, J. Electrochem. Soc., 147 (2000) 444.
24. J.H. Park, O. Ok Park, K.H. Shin, C.S. Jin, and J.H. Kim, Electrochem. Solid State Lett., 5 (2002) H7.
25. P.A. Nelson and J.R. Owen, J. Electrochem. Soc., 150 (2003) A1313.
26. M. Bursell, A. Lundblad, and P. Bjornbom, Electrochemical Society Proceedings, 7 (2002) 116.
27. V. Ganesh, and V. Lakshminarayanan, Electrochim. Acta, 49 (2004) 3561.
28. V. Ganesh, V. Lakshminarayanan, and S. Pitchumani, Electrochem. Solid State Lett., 8(6) (2005) A308.
29. I.J. Brown, S. Sotiropoulos, Electrochim. Acta, 46 (2001) 2711.
30. K.W. Nam, W. S. Yoon, K. B. Kim, Electrochim. Acta, 47 (2002) 3201.

31. K.R. Prasad, and N. Miura, Electrochem. Commun., 6 (2004) 849.
32. J.H. Chen, W.Z. Li, D.Z. Wang, S.X. Yang, J.G. Wen, and Z.F. Ren, Carbon, 40 (2002) 1193.
33. V. Subramanian, S.C. Hall, P.H. Smith, and B. Rambabu, Solid State Ionics, 175 (2004) 511.
34. K.R. Prasad, and N. Miura, Electrochem. Commun., 6 (2004) 1004.
35. B.E. Conway and W.G. Pell, J. Power Sources, 105 (2002) 169.
36. K.S. Cole and R.H. Cole, J. Chem. Phys., 9 (1941) 341.
37. J. Miller, in Proceedings of the 8th International Seminar on Double-Layer Capacitors and Similar Energy Storage Devices, Deerfield Beach, FL, Dec 7-9, 1998.
38. E. Lust, A. Janes, and M. Arulepp, J. Electroanal. Chem., 562 (2004) 33.
39. P.L. Taberna, P. Simon, and J.F. Fauvarque, J. Electrochem. Soc., 150 (2003) A292.
40. Sagar Mitra, A.K. Shukla, and S. Sampath, Electrochem. Solid State Lett., 6 (2003) A149.

Legends for the figures

1. Cyclic voltammograms obtained using porous Ni cell assemblies of (a) Symmetric supercapacitor (Porous Ni| KOH |Porous Ni) at various scan rates of a) 50, b) 100, c) 200 and d) 500 mV s^{-1} and (b) Asymmetric supercapacitor (Porous Ni| KOH |Activated carbon) at various scan rates such as a) 25, b) 50, c) 100, d) 200 and e) 500 mV s^{-1} in 6M KOH aqueous solution.

2. Cyclic voltammograms obtained using NiO cell assemblies of (a) Symmetric supercapacitor (NiO| KOH |NiO) at different scan rates such as a) 10, b) 25, c) 50, d) 100, e) 200 and f) 500 mV s^{-1} and (b) Asymmetric supercapacitor (NiO| KOH |Activated carbon) at different scan rates of a) 25, b) 50, c) 100, d) 200 and e) 500 mV s^{-1} in 6M KOH aqueous solution.

3. Variation of I/ν with different scan rates used for the capacitance measurement using cyclic voltammetry for (a) Symmetric supercapacitor of high surface area porous nickel (Porous Ni| KOH |Porous Ni). (b) Similar plots for the other cell assemblies namely (a) Asymmetric supercapacitor based on the porous nickel electrode (Porous Ni| KOH |Activated carbon). (b) Symmetric supercapacitor (NiO| KOH |NiO) and (c) Asymmetric supercapacitor (NiO| KOH |Activated carbon) based on nickel oxide electrode.

4. Nyquist plots using high surface area porous Ni as an electrode material for (a) Symmetric supercapacitor (Porous Ni| KOH |Porous Ni) at two different dc potentials of a) –1.0V and b) –0.9V and for (b) Asymmetric supercapacitor (Porous Ni| KOH |Activated carbon) at two different dc potentials of a) –1.0V and b) –0.9V in 6M KOH aqueous solution.

Inset shows the expanded high frequency region of the same plot.

5. Typical impedance (Nyquist) plots using NiO obtained from the porous Ni as an electrode material in 6M KOH aqueous solution for (a) Symmetric supercapacitor (NiO| KOH |NiO) at dc potentials of a) 0V and b) 0.1V and (b) Asymmetric supercapacitor (NiO| KOH |Activated carbon) at dc potentials of a) 0V and b) 0.1V. Inset shows the zoomed portion of the same plot at high frequency region.

6. The plots of imaginary part of the complex capacitance [$C''(\omega)$] with the frequency (in logarithmic scale) for,
   (a) Symmetric supercapacitor (Porous Ni| KOH |Porous Ni) and
   (b) Asymmetric supercapacitor (Porous Ni| KOH |Activated carbon) based on the high surface area porous nickel electrode.
   (c) Symmetric supercapacitor (NiO| KOH |NiO) and
   (d) Asymmetric supercapacitor (NiO| KOH |Activated carbon) based on the nickel oxide electrode.

7. Plots of normalized active power, |P|/|S| and reactive power |Q|/|S| vs. frequency (in logarithmic scale) for (a) Symmetric and (b) Asymmetric supercapacitor cell assemblies using the high surface area porous Ni as an electrode material.

8. Plots of normalized active power, |P|/|S| and reactive power |Q|/|S| vs. frequency (in logarithmic scale) for (a) Symmetric and (b) Asymmetric supercapacitor cell assemblies using NiO obtained from the electrochemical oxidation of porous Ni as an electrode material.

9. Representative galvanostatic charge-discharge curves for the respective devices of (a) Symmetric (Porous Ni| KOH |Porous Ni) and (b) Asymmetric (Porous Ni| KOH |Activated carbon) supercapacitor cell assemblies based on the high surface area porous Ni as an electrode material in 6M KOH aqueous solution.

10. Typical galvanostatic charge-discharge profiles of (a) Symmetric (NiO| KOH | NiO) and (b) Asymmetric (NiO| KOH |Activated carbon) supercapacitor cell assemblies based on NiO as an electrode in 6M KOH aqueous solution respectively.

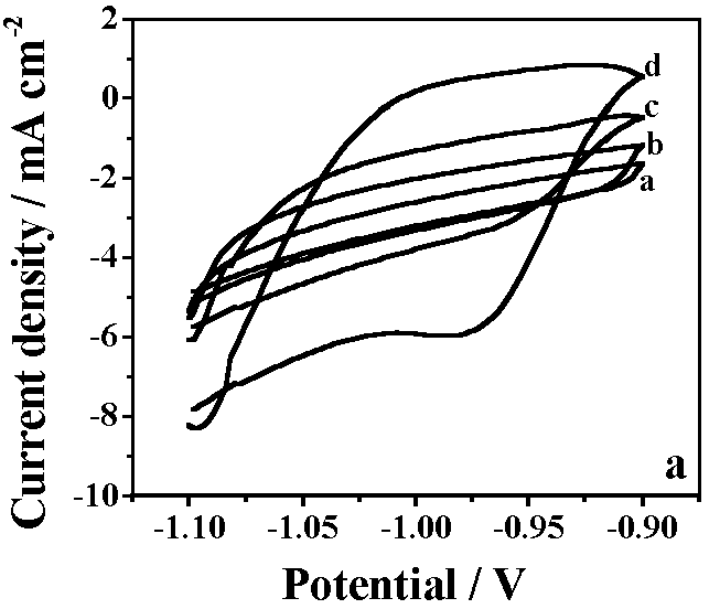
Current density / mA cm-2
2
0
-2
-4
-6
-8
-10
-1.10
-1.05
-1.00
-0.95
-0.90
Potential / V
a
d
c
b
a

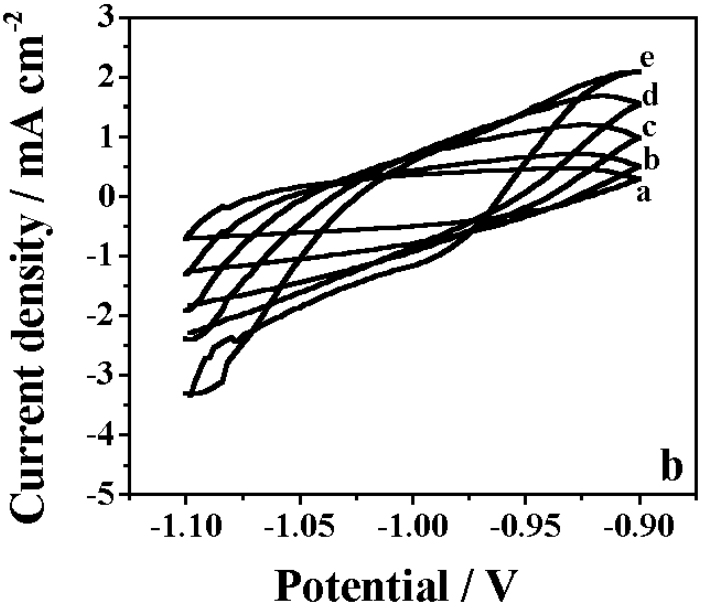
Current density / mA cm-2
3
2
1
0
-1
-2
-3
-4
-5
-1.10
-1.05
-1.00
-0.95
-0.90
Potential / V
b
e
d
c
b
a

Figure 1

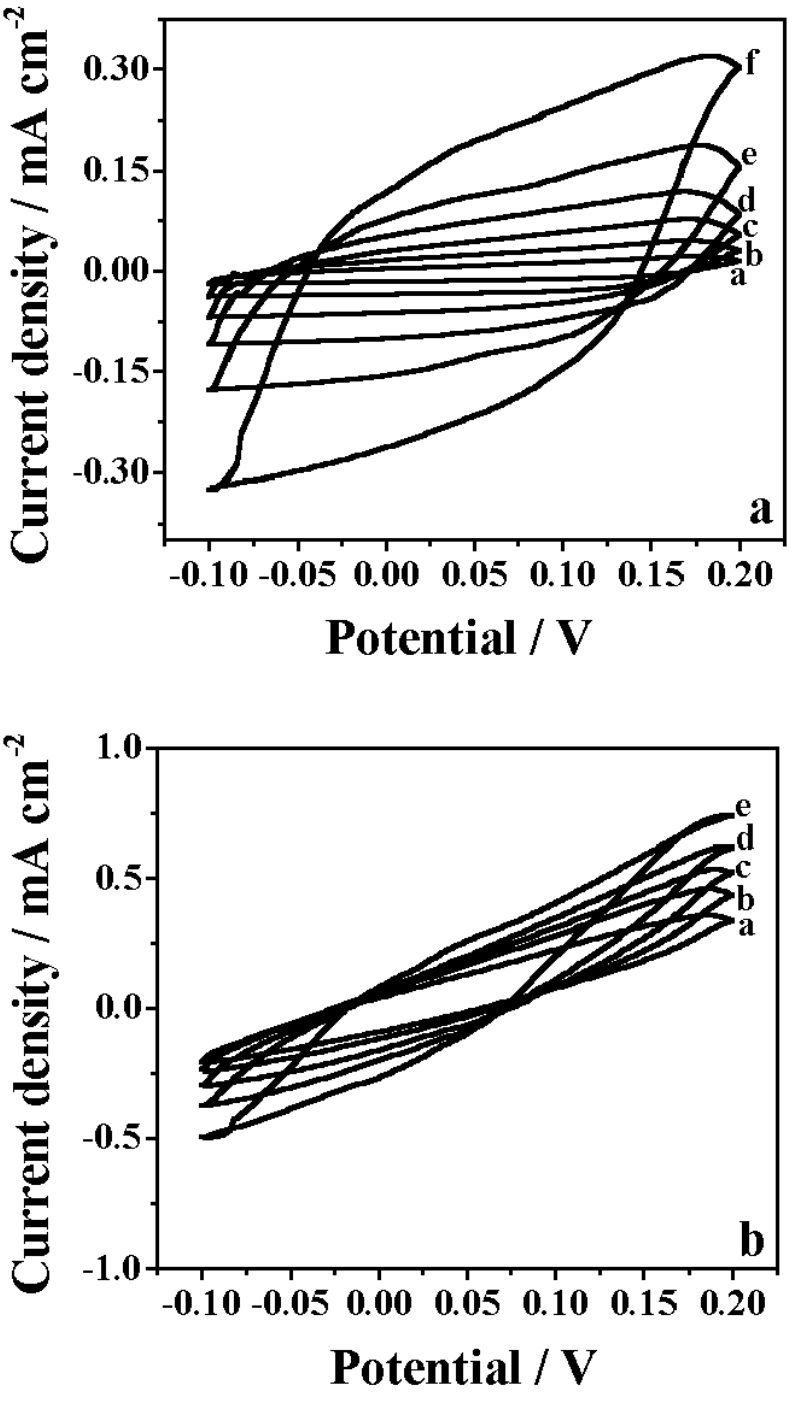
Current density / mA cm-2
0.30
0.15
0.00
-0.15
-0.30
f
e
d
c
b
a
a
-0.10 -0.05 0.00 0.05 0.10 0.15 0.20
Potential / V
Current density / mA cm-2
1.0
0.5
0.0
-0.5
-1.0
e
d
c
b
a
b
-0.10 -0.05 0.00 0.05 0.10 0.15 0.20
Potential / V

Figure 2

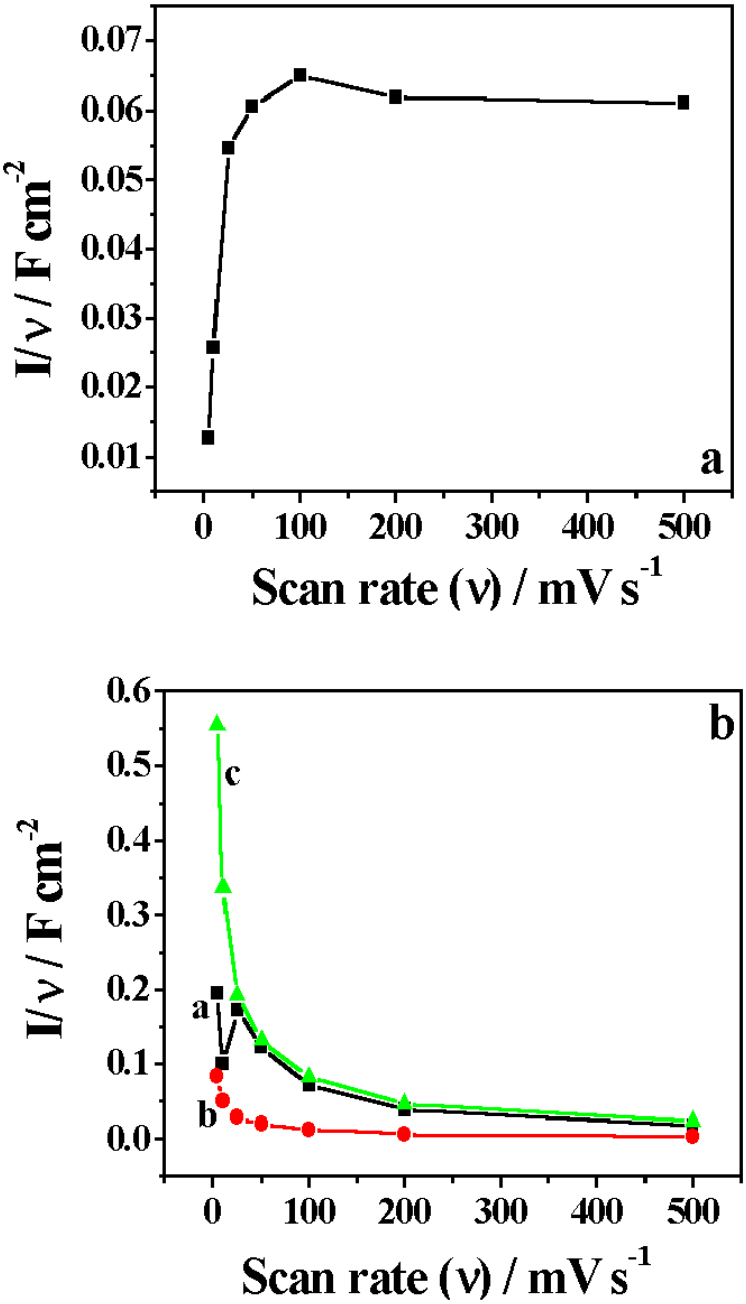
0.07
0.06
0.05
0.04
0.03
0.02
0.01
I/ν / F cm-2
a
0
100
200
300
400
500
Scan rate (ν) / mV s-1
0.6
0.5
0.4
0.3
0.2
0.1
0.0
b
c
a
b
I/ν / F cm-2
0
100
200
300
400
500
Scan rate (ν) / mV s-1

Figure 3

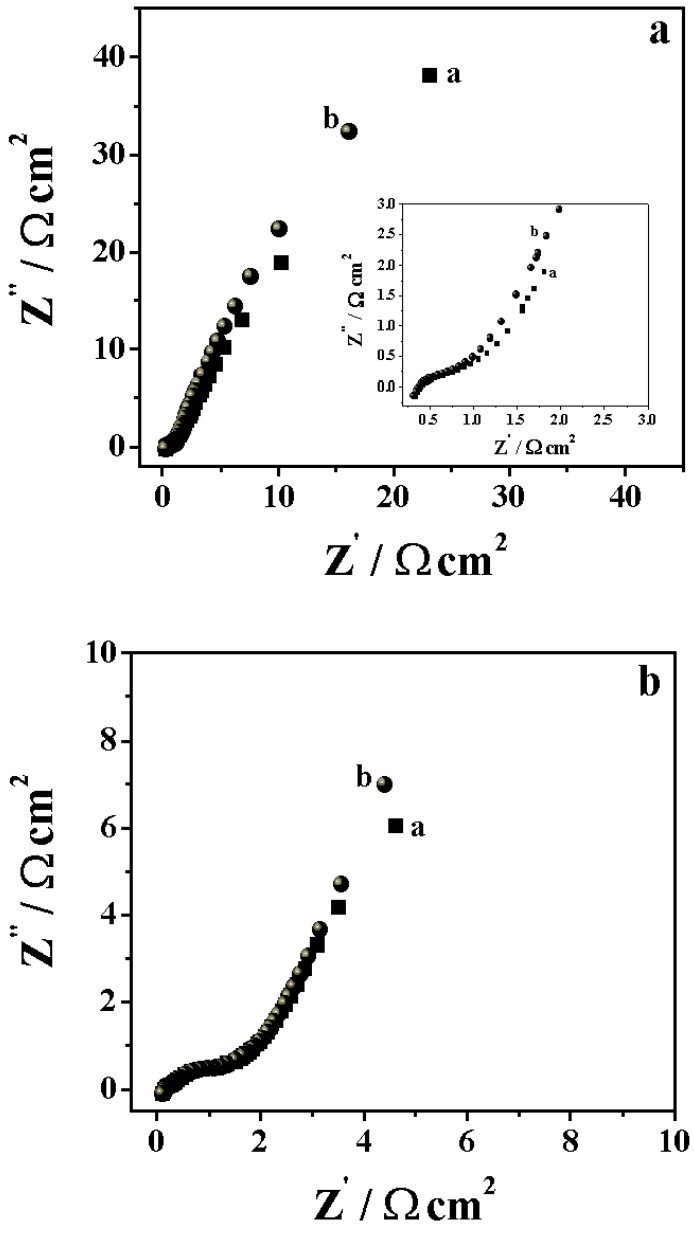
a
a
b
Z'' / Ω cm²
Z' / Ω cm²
0
10
20
30
40
b
a
Z'' / Ω cm²
Z' / Ω cm²
0.0
0.5
1.0
1.5
2.0
2.5
3.0
b
a
Z'' / Ω cm²
Z' / Ω cm²
0
2
4
6
8
10

Figure 4

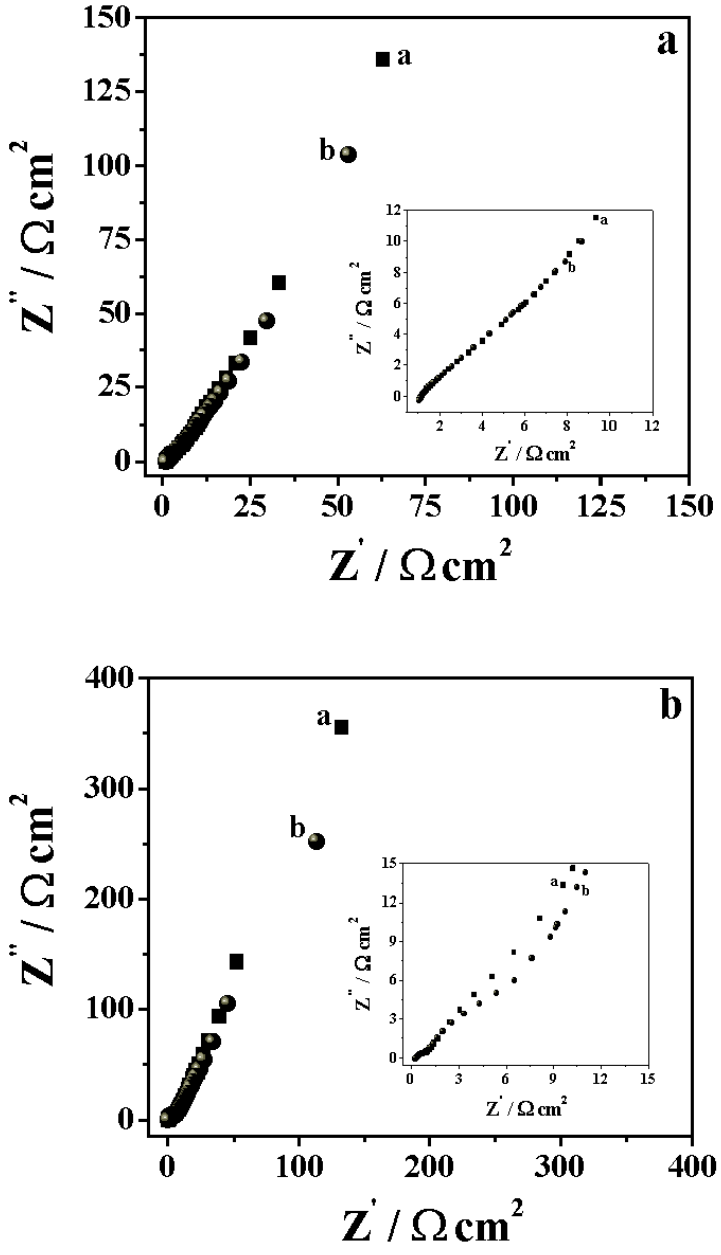
a
b
Z'' / Ω cm²
Z' / Ω cm²
0
25
50
75
100
125
150
a
b
Z'' / Ω cm²
Z' / Ω cm²
0
2
4
6
8
10
12
b
a
b
Z'' / Ω cm²
Z' / Ω cm²
0
100
200
300
400
a
b
Z'' / Ω cm²
Z' / Ω cm²
0
3
6
9
12
15

Figure 5

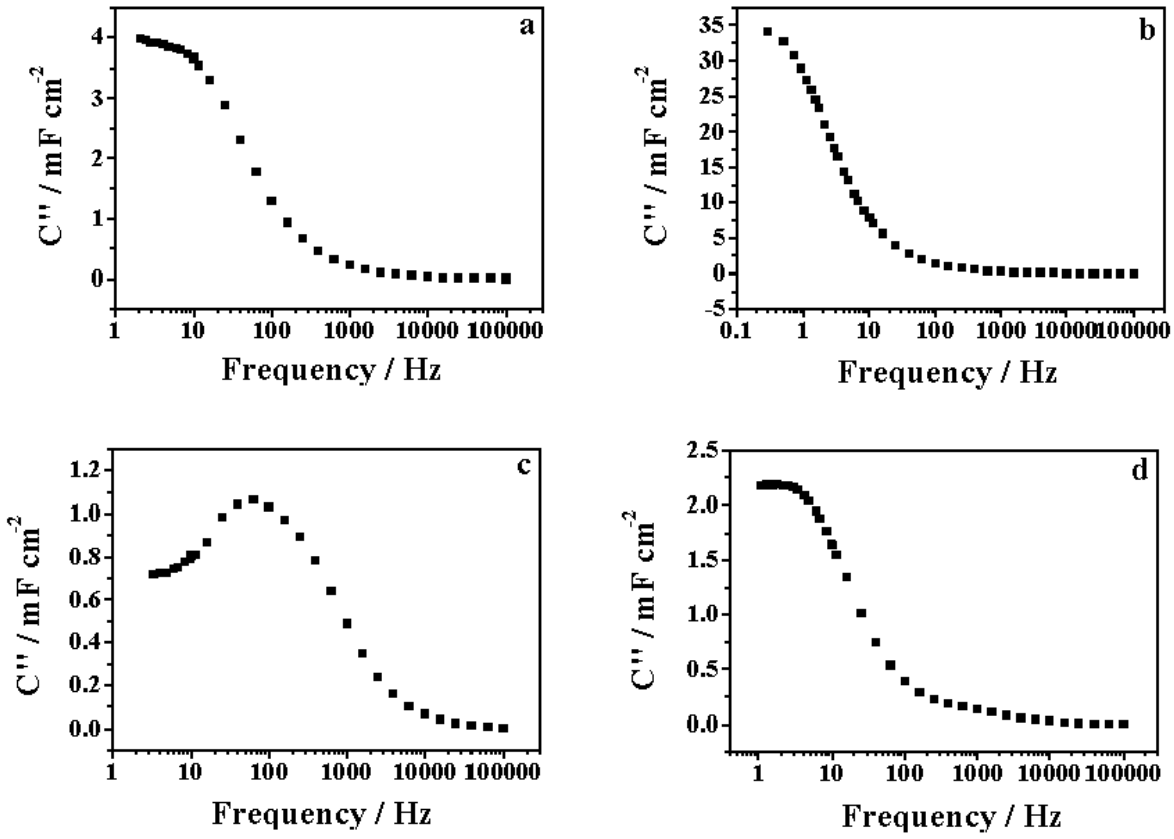
a
C'' / mF cm-2
Frequency / Hz
b
C'' / mF cm-2
Frequency / Hz
c
C'' / mF cm-2
Frequency / Hz
d
C'' / mF cm-2
Frequency / Hz

Figure 6

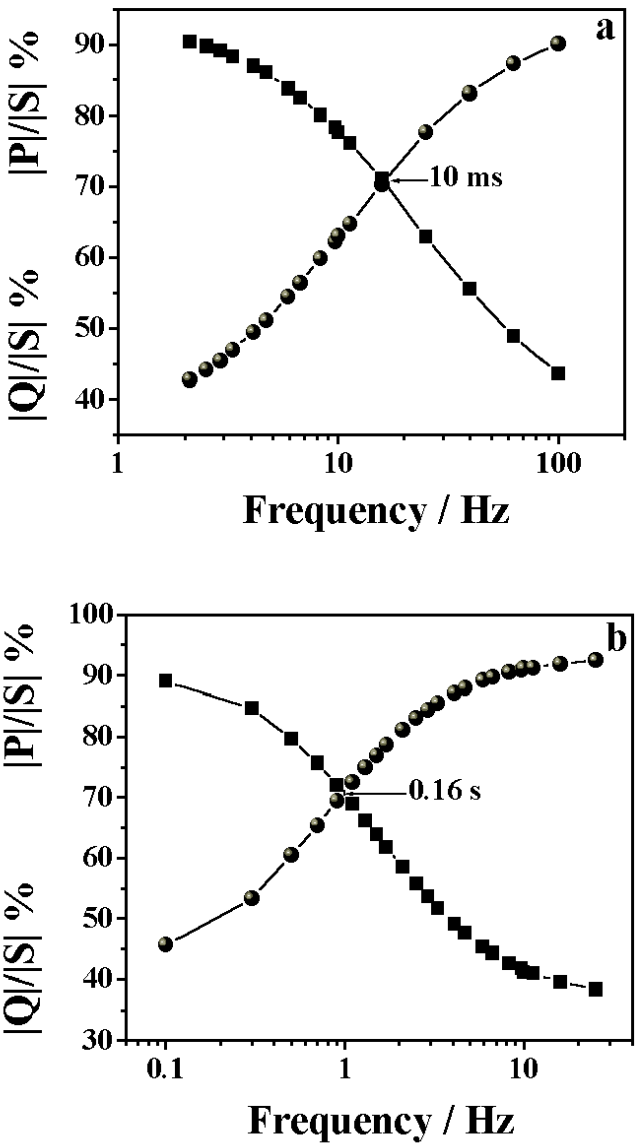
a
|P|/|S| %
|Q|/|S| %
90
80
70
60
50
40
10 ms
1
10
100
Frequency / Hz
b
100
90
80
70
60
50
40
30
0.16 s
0.1
1
10
Frequency / Hz

Figure 7

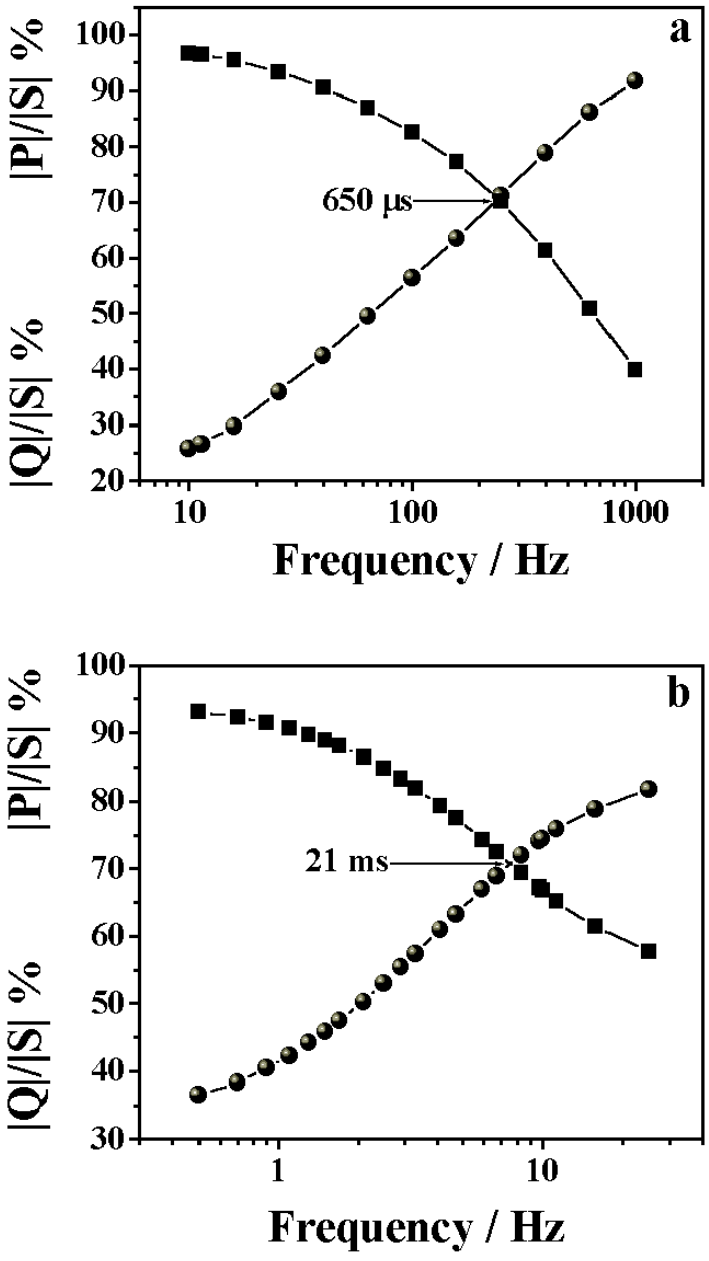

Figure 8

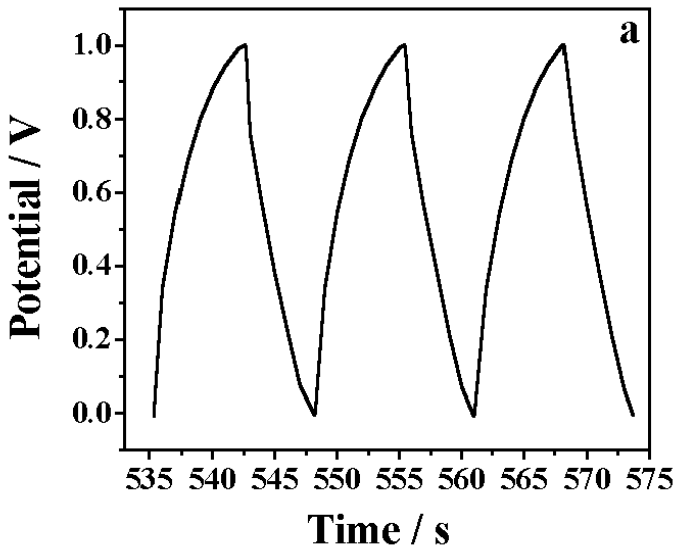
a
Potential / V
1.0
0.8
0.6
0.4
0.2
0.0
535 540 545 550 555 560 565 570 575
Time / s

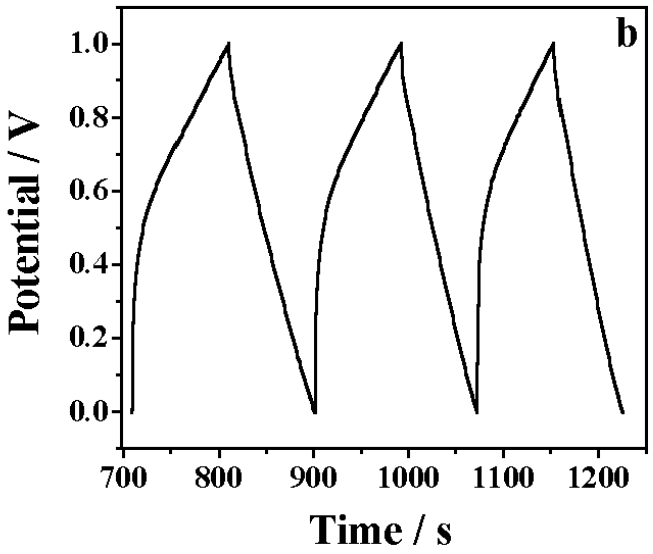
b
Potential / V
1.0
0.8
0.6
0.4
0.2
0.0
700 800 900 1000 1100 1200
Time / s

Figure 9

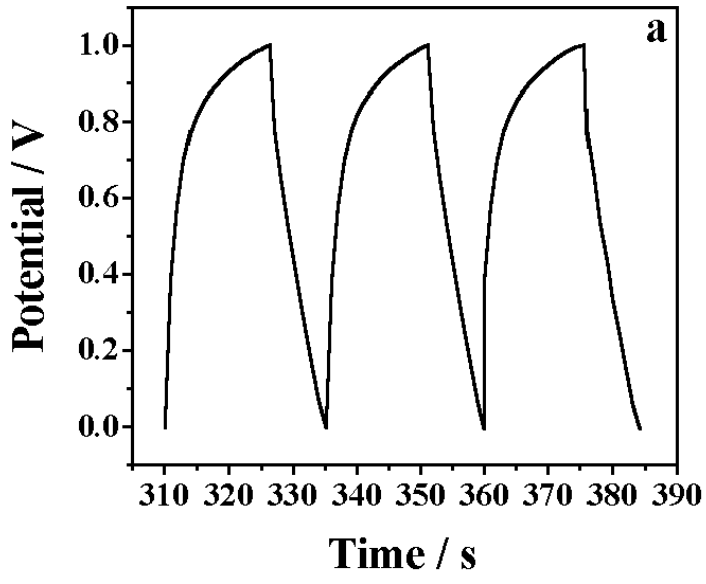
a
Potential / V
1.0
0.8
0.6
0.4
0.2
0.0
310 320 330 340 350 360 370 380 390
Time / s

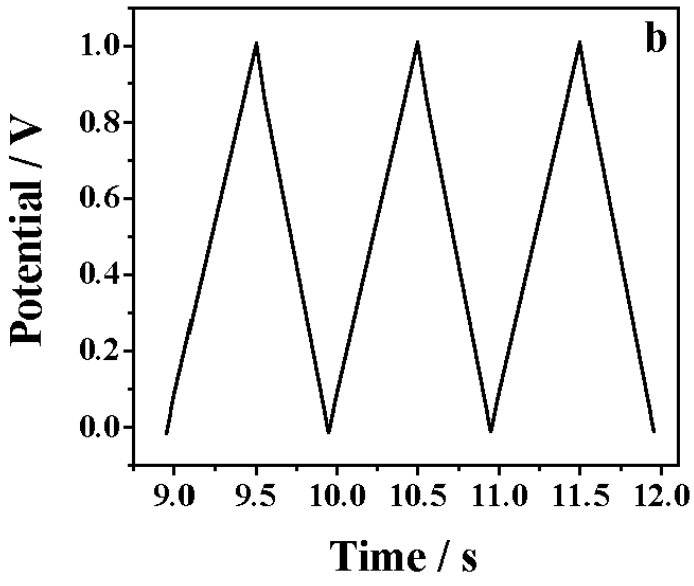
b
Potential / V
1.0
0.8
0.6
0.4
0.2
0.0
9.0 9.5 10.0 10.5 11.0 11.5 12.0
Time / s

Figure 10